



Modelling Knudsen number effects in suspension high velocity oxy fuel thermal spray

S. Chadha, R. Jefferson-Loveday, T. Hussain*

Faculty of Engineering, University of Nottingham, Nottingham, NG7 2RD, United Kingdom

ARTICLE INFO

Article history:

Received 26 September 2019

Revised 6 December 2019

Accepted 29 January 2020

Keywords:

Suspension thermal spray

SHVOF

HVSFS

Rarefied

Knudsen

Accuraspray

ABSTRACT

Suspension high velocity oxy fuel thermal spray is a system characterized by supersonic velocities and length scales of particles of the order of nm – μm . As the effects of rarefaction become significant the assumptions within the continuum models begin to collapse, the effects of rarefaction can be evaluated through the flow Knudsen number. Modifications to the numerical modelling must be made to incorporate the effects of rarefaction. This study looks to include the effects of rarefaction into the computational fluid dynamics (CFD) models for the suspension high velocity oxy-fuel (SHVOF) thermal spray process. A model for the heat transfer coefficient that take into account the Knudsen and Mach number effects is employed. Finally, the Ranz-Marshall correlation for the Nusselt number is compared to the Kavanau correlation and a compressible Nusselt number correlation. The model is validated through comparisons of particle temperatures which are obtained from two colour pyrometry measurements using a commercially available Accuraspray 4.0 diagnostic system. This study shows that there is a significant improvement in the prediction of inflight particle temperatures when accounting for the effects of compressibility and the effects of rarefaction on the Nusselt number.

© 2020 The Authors. Published by Elsevier Ltd.

This is an open access article under the CC BY license. (<http://creativecommons.org/licenses/by/4.0/>)

1. Introduction

Suspension high velocity oxy fuel thermal (SHVOF) spray is a method of deposition of nanoparticles onto the surface of a substrate to form a protective coating. Typically, in SHVOF thermal spray premixed fuel and oxygen is injected into a combustion chamber where the mixture undergoes combustion. The suspension is then injected axially into the combustion chamber where it undergoes primary breakup, secondary breakup and evaporation. The particles within the suspension are released into the gas flow where they are heated and accelerated and finally the nanoparticles are deposited onto the surface of a substrate forming a coating.

There is a significant body of modelling literature investigating what effect varying different parameters have within SHVOF thermal spray. Tabbara et al. [1] looked at injecting water droplets into the combustion chamber, to investigate the effect the initial droplet diameter has on the evaporation rate. Mahrukh et al. [2–4]. looked at the effect different axial injection types, models for suspension properties and the effect of an atomization model on the droplet breakup and evaporation rates. Taleby et al. [5] inves-

tigated the effect of gas flow rate, suspension flow rate, droplet diameter and the droplet velocity for an axial injection of ethanol droplets. Jadidi et al. [6]. looked to compare inflight particle velocities and temperatures to that of experimentally obtained values [7] from the Accuraspray G3 diagnostic system from Technar (Saint-Bruno-de-Montarville, Canada) [8]. Jadidi's SHVOF thermal spray model found a discrepancy between the Ranz-Marshall correlation and the Accuraspray measurements by approximately by 500 K.

The aim of this study is to evaluate the effectiveness of three different Nusselt number correlations in order to better predict inflight particle temperatures. With more applicable Nusselt number correlations this study aims to address the underprediction for inflight particle temperatures reported within SHVOF literature. For the numerical model, commercial CFD software Ansys Fluent V19.0 [9,10] (Pennsylvania, USA) is employed. The numerical model is validated using a two colour pyrometry measurements of the inflight particle velocity and temperature. For the experimental investigation the Accuraspray 4.0 system from Technar (Saint-Bruno-de-Montarville, Canada) is employed to obtain inflight velocity and temperature measurements of the particles. The inflight particle velocities and temperatures from CFD are compared to the experimental measurements obtained by Accuraspray 4.0.

* Corresponding author.

E-mail address: Tanvir.Hussain@nottingham.ac.uk (T. Hussain).

Nomenclature

A	Surface area
C_1	Calibration constant ($9.352 \times 10^{-7} \text{ w.m}^{-2}$)
C_2	Calibration constant ($1.439 \times 10^{-12} \text{ m.k}$)
c_p	Specific heat capacity
d	Diameter
h	Heat transfer coefficient.
$h_{\text{vap},i}$	Latent heat i^{th} species
I	Intensity
k	Thermal conductivity
Kn	Knudsen Number
L	Latent heat of fusion
m	Mass
Ma	Mach number
Nu	Nusselt number
Nu_0	Incompressible Nusselt number
Pr	Prandtl number
Re	Reynolds number
T	Temperature
t	Time
\vec{u}	Velocity
ρ	Density
μ	Dynamic viscosity
γ	Ratio of specific heats
λ	Wavelength
Λ	Molecule mean free path
ε	Emissivity

Subscript

d	Particle at diameter
i	Species
∞	Gas
p	Particle

To determine the temperature of particles within SHVOF thermal spray it is necessary to determine the particle heat transfer coefficient. Traditionally in SHVOF thermal spray modelling the analysis on the heat transfer coefficient is computed from the Ranz-Marshall [11] correlation for the Nusselt number. The Ranz-Marshall correlation was developed from droplet evaporation experiments at low Reynolds numbers and low Mach numbers for application to spray drying [11,12]. Experiments to determine the heat transfer coefficient and the evaporation rate of droplets were conducted at varying Reynolds numbers from 0 – 200. The popularity of this correlation arose from its simplicity and the fact that it was stated that the correlation extrapolates well five times above the range of Reynolds numbers at which the experiments were conducted, however the results for this claim were not corroborated within the paper [11]. The Ranz-Marshall correlation does not account for the Mach number effects on the heat transfer to particles. SHVOF thermal spray is a process characterised by gas velocities within the range of 1250 – 1750 m/s and gas temperatures within the range of 2200 K – 3500 K. A characteristic feature of SHVOF thermal spray are the shock diamonds witnessed within the free jet region as the flow is under expanded at exit. The effects of compressibility alter the behaviour of the flow for particle laden flows and hence must be evaluated.

The Knudsen number, Kn, can be used to evaluate the effects of rarefaction on a flow. As the Knudsen number increases the effects of rarefaction become significant and non-continuum effects must be considered. For particle laden flows, as the Kn number increases into the slip flow regime, the first observable non continuum effect occurs on the surface of the particles. A temperature and velocity jump is apparent on the surface of

particles [13]. As the Knudsen number increases further into the free molecular flow regime there is no interaction between gas molecules approaching the surface of the particles and those leaving the surface. Hence, the gas molecules arriving at a surface will have the full freestream velocity. Fig. 1 distinguishes the different flow regimens within rarefied flows it also shows the change in the flow profile on the particle surface for the different regimes.

$$Kn = \frac{\Lambda}{d_p} \approx \sqrt{\frac{\pi \gamma}{2}} \left(\frac{Ma}{Re_p} \right) \quad (1)$$

Kavanau et al. [14] derived the heat transfer coefficient of spherical particles within the slip flow regime and derived a Nusselt number correlation for application to particles within a rarefied gas flow. Kavanau provided an alternative Nusselt correlation that accounts for the effect of rarefaction on the Nusselt number, which is given by Eq. (5) in the modelling section (2). The correlation proposed by Kavanau et al. asymptotically approaches the value predicted by Sauer et al. [15] for free molecular flow for large Kn [16]. Drake et al. measured the heat transfer coefficient for particles within a rarefied gas in supersonic flow [17]. The data by Drake et al. has been compared to the correlation by Kavanau et al. and the correlation is shown to fit well to particles within a rarefied supersonic flow as well as subsonic flows. The correlation was plotted against experimental measurements for the Nusselt number for particles in a rarefied gas in supersonic conditions. The results from Drake et al. and Kavanau et al. with varying flow Mach number from 0.10 – 6.0 are provided within Fig. 2. An alternative Nusselt correlations to the Ranz-Marshall and Kavanau correlation has been applied to cold spray and high velocity oxy fuel thermal spray (HVOF); however, it has not yet been employed within SHVOF thermal spray. The compressible correlation provides the Nusselt number as a function of the Mach number. There are a number of Nusselt correlations available in literature; however, SHVOF thermal spray has solely used the Ranz-Marshall correlation comparing the correlation to other available Nusselt number correlations within literature [2,5,18–20].

2. Numerical Modelling

A fully structured 3-D mesh of 2.25 million cells is employed to model the fluid domain. The premixed fuel and air are injected into the combustion chamber using an annular inlet located 4 mm from the centre of the combustion chamber and with a width of 1 mm. A steady state gas flow field is established before injecting the suspension, the suspension is comprised of 80 wt percent of water and 20 wt percent of Cr_2O_3 . To model the gas phase the continuity, momentum conservation, ideal gas law, energy conservation, species fraction and the realizable $k-\varepsilon$ turbulence model with an enhanced wall function are solved for using the SIMPLE algorithm and the QUICK scheme for the convective terms [3]. The details of the governing equations have been omitted and can be found in our prior studies [21,22]. The combustion reaction is modelled using the eddy dissipation concept (EDC) model along with a detailed reaction mechanism to model the combustion, the reaction mechanism along with its associated chemical kinetics can be found within our prior study [22]. The boundary conditions for the gas phase and the discrete phase are outlined in Table 1.

The discrete phase is injected using a two-way coupled discrete particle model (DPM) model with a multicomponent injection [23]. The discrete particle model treats the droplets as point entities which are typically much smaller than the mesh resolution. Hence with this approach the boundary layer around the particles is not resolved and instead the boundary layer effects are taken into account through the drag and Nusselt number correlations. A multicomponent injection is a droplet comprised of N species. The discrete particle model makes the following assumptions [10]:

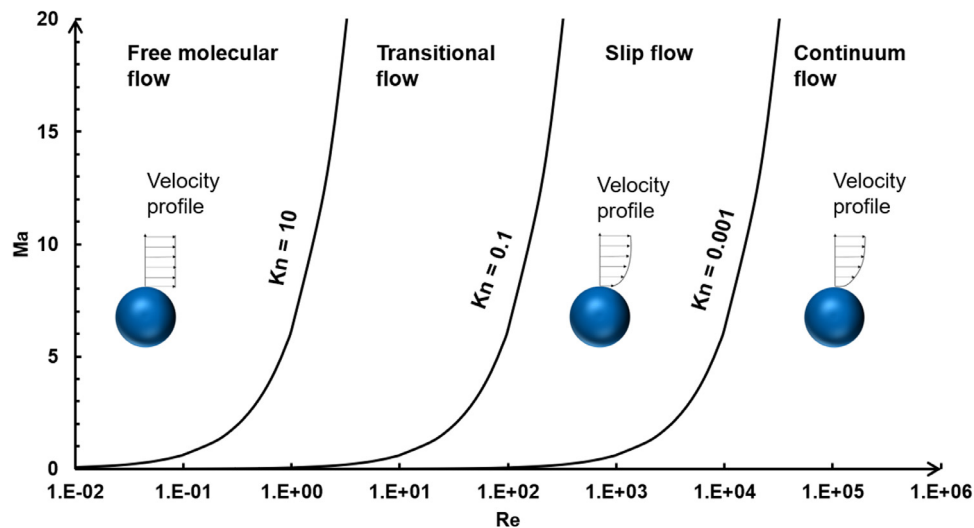


Fig. 1. Effect of Knudsen number on different flow regimes adapted from [13].

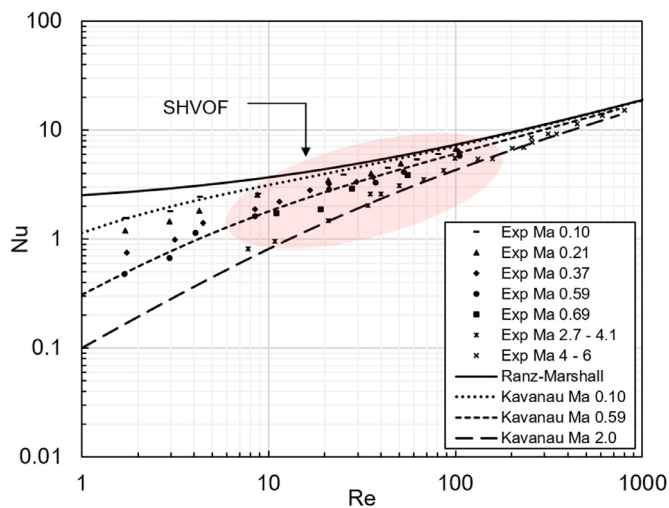


Fig. 2. Convective heat transfer coefficient for a sphere in a rarefied gas at varying Mach numbers fitted to incompressible theory and rarefied theory reproduced from [14].

Table 1

Boundary conditions employed within the model.

Parameters	Values	Temperature
Total Gas Flow Rate	0.0059 Kg/s	300 K
H ₂ vol Flow Rate	440 l/min	
O ₂ vol Flow Rate	220 l/min	
Outlet Condition	Pressure Outlet	300 K
Equivalence Ratio	1	
Suspension Flow Rate	50 ml/min	300 K
Wall Boundary Condition		500 K
Inlet Turbulence Intensity	10%	
Inlet Turbulent Length Scale	7×10^{-5} m	

- The discrete phase is dilute such that particle-particle interactions are negligible.
- The effects of the discrete phase on the continuous phase are small and are accounted through source terms within the mass, momentum and energy equations.
- Discrete particles are modelled as uniform point entities.
- Discrete particles are modelled as spherical bodies.

The properties of the droplet such as the specific heat and density are calculated from the volume average of the various constituent components. The viscosity is calculated using the correlation proposed by Guth et al. [24] to include the effect of the nanoparticles on the viscosity of the droplet. The surface tension is given by the surface tension of water below the boiling point of water, and above the melting temperature of Cr₂O₃ the surface tension for molten Cr₂O₃ is employed. The thermal physical properties of water and Cr₂O₃ are given in Tables 2 and 3 respectively. Further information on the governing equations can be found in our prior study [21].

To model the liquid jet the “blob” method has been employed [25] which is one of the most popular approaches found in literature due to its simplicity. The jet injection is reduced to an injection of “blobs” with an equivalent diameter of the injector. The blobs are subject to secondary breakup and evaporation. The cone injection type consisting of 20 particle streams has been employed for the suspension injection. A cone angle of 2.6° has been calculated based upon the research of Ranz [26]. The two-way turbulence coupling model has been employed to account for the effect of the particles on the turbulent kinetic energy field [22]. At large Weber numbers the droplet breakup can be characterised by the KHRT breakup model [1]. The KHRT breakup model assumes the breakup time and droplet sizes are related to the fastest growing Kelvin-Helmholtz instabilities on the droplet surface within the liquid core. Outside of the liquid core it is assumed that breakup is driven by the aerodynamic forces from the adjacent flow field, which results in the Rayleigh-Taylor instabilities facilitating the breakup of the droplets. The pressure dependant boiling sub-model has been employed to account for the effect of the pressure variation within the combustion chamber on the evaporation of the suspension. The unsteady discrete phase is solved for every 10 gas phase iterations with a DPM time step of 1×10^{-5} s. The inverse distance node-based averaging of the source term is employed to distribute the DPM source term amongst neighbouring cells [27].

The motion of the droplets is given by Newton’s second law, the significant force acting on the particles being the drag force. The drag coefficient, C_D , is given by the correlation by Crowe [28] which considers the effect of the Mach number, Ma , and the Reynolds number, Re , on the drag coefficient [6]. The particle temperature, T , can be determined from a heat balance assuming no internal temperature gradient within the droplet. The energy equation for the multicomponent droplet is given by Eq. (2). Where m_p refers to the mass of the particle, h , refers to the heat transfer

Table 2
Thermo-physical properties; density, viscosity, specific heat and surface tension of water [3].

Property	Water Temperature dependant Functions	Temperature range (K)
Density (kg/m ³)	$\rho_l = aT^2 + bT + c$ $a = -0.003$ $b = 1.5078$ $c = 815.88$	290 - 373
Viscosity (Kg/m.s)	$\mu_l = aT^2 + bT + c$ $a = 1.09 \times 10^{-7}$ $b = -8.11 \times 10^{-5}$ $c = 0.0153$	290 - 373
Specific Heat (J/kg.K)	$Cp_l = aT^3 + bT^2 + cT + d$ $a = -2.45 \times 10^{-5}$ $b = 0.034$ $c = -14.02$ $d = 5993.1$	290 - 373
Thermal Conductivity (W/m.K)	$k = aT^2 + bT + c$ $a = 9.67 \times 10^{-5}$ $b = 0.0074$ $c = 0.7511$	250 - 385
Surface Tension (N/m)	$\sigma_l = aT^2 + bT + c$ $a = -2.52 \times 10^{-7}$ $b = -5.41 \times 10^{-6}$ $c = 0.096$	290 - 373

Table 3
Thermo-physical properties of Cr₂O₃ [38].

Property	Values	Temperature range (K)
Density (kg/m ³)	$\rho = 5520$	
Specific Heat (J/kg.K)	$Cp = a + bT$ $a = 715.73$ $b = 0.11011$ $Cp = 83,225$ $Cp = 1032$	273 - 2705 2705 - 2715 2715 +
Thermal Conductivity (W/m.K)	22.22	
Surface Tension (N/m)	$\sigma = 0.812$	2710 +

coefficient, A_p refers to the surface area of the particle, T_∞ refers to the gas temperature, $h_{vap,i}$ refers to the latent heat of vaporisation and the rate of change of $\frac{dm_i}{dt}$ refers to the evaporation rate. The heat transfer coefficient is computed from the Nusselt number, Nu , the particle diameter, d_p and the thermal conductivity of the gas, k_∞ which is shown in Eq. (3). For this investigation three different Nusselt correlations are evaluated. The Ranz-Marshall correlation determines the Nusselt number from the Reynolds number and the Prandtl number, Pr , which is given by Eq. (4).

$$m_p c_p \frac{dT}{dt} = h A_p (T_\infty - T_p) + \sum_i \frac{dm_i}{dt} (h_{vap,i}) \quad (2)$$

$$h = \frac{Nu k_\infty}{d_p} \quad (3)$$

$$Nu = 2.0 + 0.6 Re_p^{0.5} Pr^{1/3} \quad (4)$$

The Kavanau correlation [29] accounts for the effects of rarefaction and high Mach number effects on the Nusselt correlation, this model is given by Eq. (5). The Ranz-Marshall correlation is employed for the incompressible Nusselt number, Nu_0 .

$$Nu = \frac{Nu_0}{1.0 + 3.42 Nu_0 \frac{Ma}{Re_p Pr}} \quad (5)$$

An additional correlation for the Nusselt number that is often used in HVOF and cold spray modelling but has not yet been applied to SHVOF provides the Nusselt number as a function of the Mach number. The compressible correlation [30] which accounts for the effects of Mach number but not that of rarefaction on the heat transfer and is given by Eq. (6). This expression is valid for

cases where the Mach number exceeds 0.24 and the gas temperature is greater than the particle temperature. The particle Reynolds number and the gas Prandtl number are given by Eq. (7) and 8 respectively. Where ρ refers to the density of the gas, $(\bar{u}_p - \bar{u})$ refers to the magnitude of the difference of the particle velocity and gas velocity respectively and μ refers to the dynamic viscosity of the gas.

$$Nu = 2.0 + 0.4 Re_p^{0.5} Pr^{1/3} \exp(0.1 + 0.872 Ma) \quad (6)$$

$$Re = \frac{\rho d_p |\bar{u}_p - \bar{u}|}{\mu} \quad (7)$$

$$Pr = \frac{c_p \mu}{k_\infty} \quad (8)$$

To account for the melting an effective specific heat capacity model is employed. The effective specific heat capacity method adjusts the specific heat capacity, c_p , to account for the latent heat of fusion, L , required to melt solid Cr₂O₃. The effective specific heat capacity is calculated using Eq. (9) [31,32] where the subscripts s and l refer to the specific heat capacity for the solid and liquid phases respectively.

$$c_p = \begin{cases} c_{pCr_2O_3s}, & T < T_1 \\ \frac{1}{2} \left(\frac{L}{T_2 - T_1} + c_{pCr_2O_3s} + c_{pCr_2O_3l} \right), & T_1 \leq T < T_2 \\ c_{pCr_2O_3l}, & T \geq T_2 \end{cases} \quad (9)$$

3. Experimental Methodology

The inflight particle velocities and temperatures are measured using the Accuraspray 4.0 device (Technar, Saint-Bruno-de-Montarville, Canada) [8]. The Accuraspray system measures the ensemble average of the inflight particle velocity and temperature. Fig. 3 shows the Accuraspray system in operation with the SHVOF thermal spray gun. The measurements are taken using a two colour pyrometer that evaluates the radiation intensity from the particle at two wavelengths. Planks law describes the radiation emitted from a body which is given by Eq. (10). Where, I , refers to the radiation intensity at a wavelength, λ , for a body at temperature, T , with an emissivity, ε , C_1 and C_2 are calibration constants. The radiation intensity is measured at two wavelength (λ_1 and λ_2) and the temperature can be determined from Eq. (11) [33].

$$I(\lambda, T) = \varepsilon \frac{C_1}{\lambda^5} \frac{1}{\exp\left(\frac{C_2}{\lambda T}\right) - 1} d\lambda \quad (10)$$



Fig. 3. Accuraspray 4.0 system in operation with an SHVOF thermal spray gun.

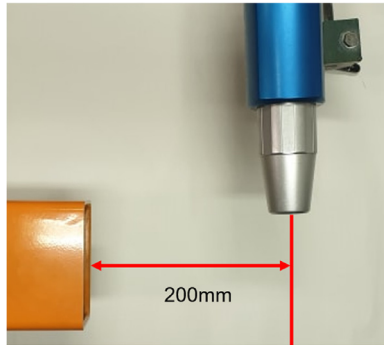


Fig. 4. Accuraspray 4.0 positioning to the SHVOF thermal spray gun.

$$T = \frac{C_2(\lambda_1 - \lambda_2)}{\lambda_1 \lambda_2} \left[\ln \left(\frac{\lambda_1}{\lambda_2} \right) + 5 \ln \left(\frac{\lambda_1}{\lambda_2} \right) \right]^{-1} \quad (11)$$

The particle velocity is determined using a “time of flight” approach [34], where the radiation emitted from the particles is detected at two locations parallel to the direction of travel of the particles. The distance between the two measurement locations is known and hence from the time delay between the two corresponding signals the velocity can be determined [33].

The Accuraspray sensor is placed at the measurement locations (75, 100, 125 and 150 mm) downstream from the SHVOF gun exit. The sensor is placed at a distance of 200 mm radially from the jet axis [35] as shown in Fig. 4. A 75-kW flame is established with the flow rates outlined within table one and a suspension comprised of 80% H₂O and 20% Cr₂O₃ is injected at a flow rate of 50 ml/min into the centre of the combustion chamber, the Neoxid (C101S) suspension was obtained from Millidyne (Finland). The particle size distribution for Cr₂O₃ within the suspension is given by Fig. 5. The particle size distribution in the suspension was measured with a laser diffraction technique. The measurements for the inflight particle velocity and temperature are obtained at the various standoff distances.

4. Results and discussion

Fig. 5 shows the particle size distribution for Cr₂O₃ within the suspension. Two peaks are seen within the distribution as one peak correlates to the non-agglomerated particle distribution, nominal particle size from the supplier is 500 nm which corresponds to the initial peak. The second peak corresponds to particles that have agglomerated within the suspension. Fig. 6 shows the centerline gas temperature predicted by the Ranz–Marshall, Kavanau and the compressible correlations. From Fig. 6, it can be seen that both the Kavanau and the compressible correlation predict a very similar temperature while the Ranz–Marshall correlation predicts a significantly higher gas temperature within the combustion chamber and a lower gas temperature within the

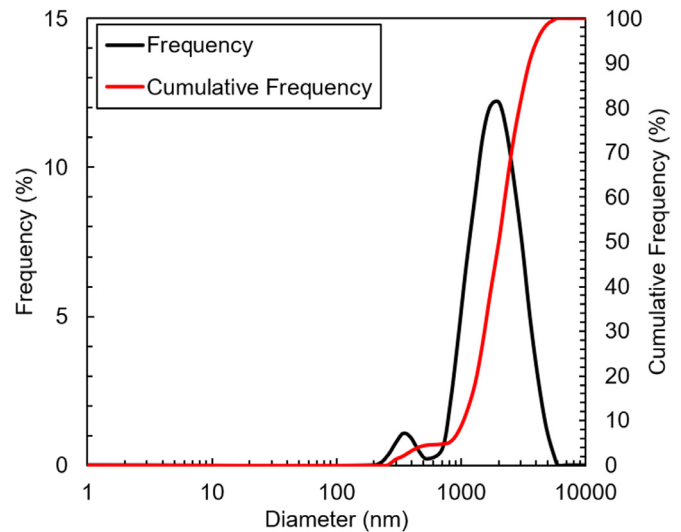


Fig. 5. Particle size distribution of Cr₂O₃ particles in the suspension.

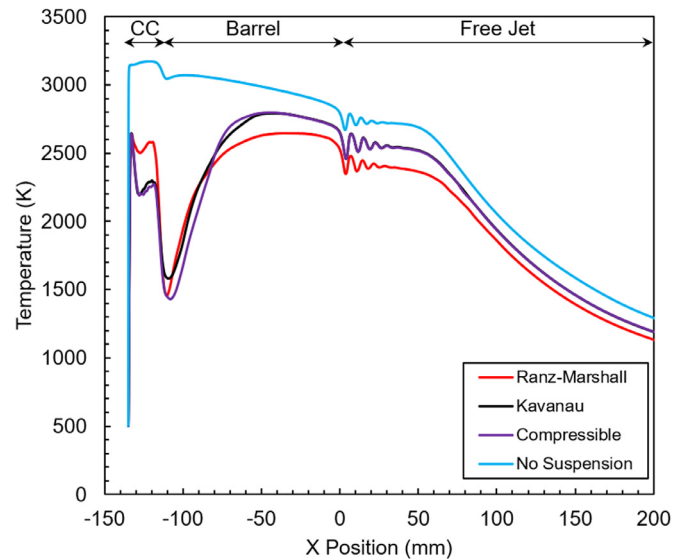


Fig. 6. Centreline Gas temperature for the three Nusselt correlations evaluated.

barrel and the free jet. The heat transferred to the suspension is proportional to the heat transfer coefficient, Eq. (2). Kavanau et al. [14], Drake et al. [17] evaluated the heat transfer coefficient to particles within high Mach flows. These studies demonstrated that the incompressible correlations for the Nusselt number such as the Ranz–Marshall correlation overestimate the heat transfer coefficient. An overestimate of the heat transfer coefficient will result in a lower delayed evaporation rate and hence higher gas temperatures within the combustion chamber and will over predict the heat removed from the gas and hence a lower gas temperature within the barrel and the free jet.

Fig. 7 shows the centerline evaporation rate predicted by the Ranz–Marshall, Kavanau and Compressible correlations. From Fig. 7, it can be seen again that a very similar evaporation rate profile is predicted by the Kavanau and the compressible correlation. Both the correlations predict a maximum centreline evaporation rate within the combustion chamber of approximately 4.2×10^{-8} kg/s. While the Ranz–Marshall correlation predicts a lower maximum evaporation rate of under 2.0×10^{-8} kg/s. In addition to this, it can be seen from Fig. 7 that the compressible correlation predicts evaporation to commence soonest at a distance of

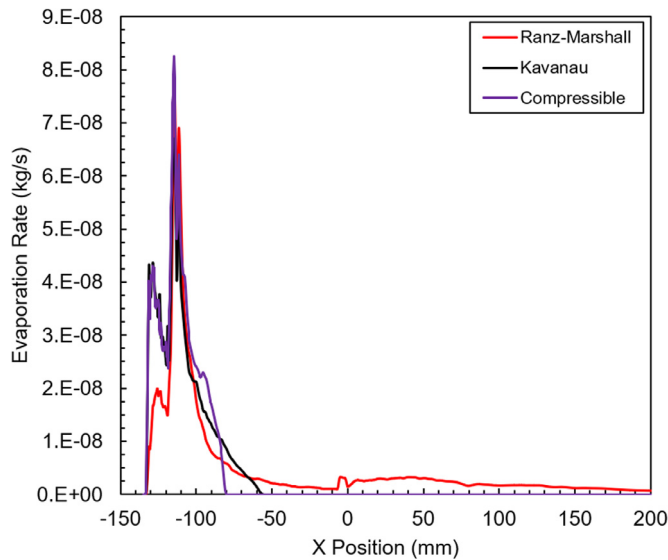


Fig. 7. Centreline evaporation rates for the three Nusselt correlations evaluated.

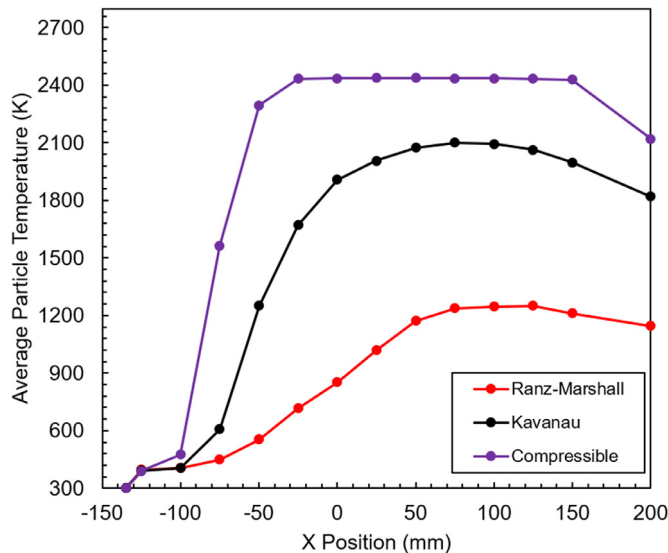


Fig. 8. Average inflight particle temperatures for the three Nusselt correlations considered, particle temperatures were averaged at the locations indicated on the graph by the points.

80 mm (inside the nozzle) from the nozzle exit. The Kavanau correlation predicts evaporation to commence at 60 mm (inside the nozzle) from the nozzle exit. While the Ranz–Marshall correlation predicts the evaporation to continue all the way to 200 mm (outside the nozzle) from the nozzle exit. Typical standoff distance for SHVOF thermal spray is 85 mm from the nozzle exit and hence this correlation predicts that moisture will still be present within the particles as they deposit onto a substrate. The reduction in the gas temperature within the free jet region seen in Fig. 6 for the Ranz–Marshall correlation is in large part a result of the heat requirement to vaporize the liquid.

Fig. 8 show the average inflight particle temperature predicted by the three different Nusselt correlations. It can be seen from Fig. 8 that the compressible correlation predicts the highest average particle temperature and lowest average particle temperature is predicted by the Ranz–Marshall correlation. This corresponds to the evaporation rate where both the model predicting evaporation to commence soonest results in the highest particle temperature.

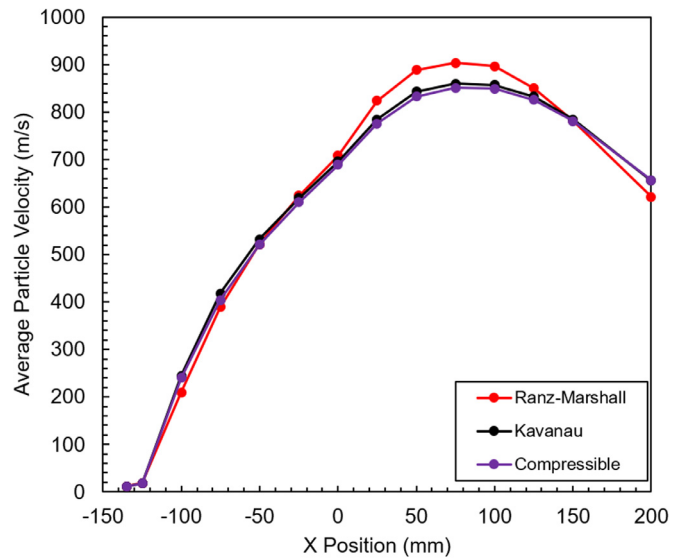


Fig. 9. Average inflight particle velocities for the three Nusselt correlations considered, particle velocities were averaged at the locations indicated on the graph by the points.

The compressible correlation allows the particles more time for heating as evaporation commences earliest and hence predicts the highest temperature. The Ranz–Marshall correlation predicts evaporation to commence later than the other two correlations which leaves the shorter duration for particle heating. Hence, the Ranz–Marshall correlation predicts the lowest average inflight particle temperatures.

Fig. 9 show the average inflight particle velocities predicted by the three different Nusselt correlations. It can be seen from Fig. 9 that the Kavanau and compressible correlation predict a very similar inflight particle velocity. While the Ranz–Marshall correlation deviates from the other two correlations within the free jet. The effect of the Nusselt number does not affect the particle trajectory to any significant degree. This is expected as particle trajectories are largely determined by the turbulent fluctuations within the velocity field and do not depend upon the Nusselt number correlation.

Fig. 10(a), (b) and (c) shows the particle temperature distribution predicted from the Ranz–Marshall (a), Kavanau (b) and the compressible (c) correlations at 85 mm from the nozzle exit. Comparing the particle temperature distribution for the Ranz–Marshall (a), Kavanau (b) and the compressible (c) correlations it can be seen that there are drastically different particle distributions predicted by the three correlations. The Ranz–Marshall correlation predicts the widest range of particle temperatures; the model predicts particle temperatures ranging from 1000 K up to 2500 K. The Kavanau correlation predicts a particle temperature distribution ranging from 1800 K – 2500 K. The compressible correlation predicts a very narrow particle temperature distribution predicting all particles have a temperature of around 2400 – 2500 K.

Fig. 11(a), (b) and (c) shows the particle liquid mass fraction distribution predicted from the Ranz–Marshall (a), Kavanau (b) and the compressible (c) correlations at 85 mm from the nozzle exit. Comparing the distribution of the mass fraction it can be seen that the distribution predicted from the Ranz–Marshall correlation differs significantly from the other two correlations. The Ranz–Marshall correlation predicts that over 50% of the particles will have some moisture retained within the droplet upon impacting the substrate. The significantly lower average temperature seen by the Ranz–Marshall correlation in Fig. 10 is a result of the high degree of particles that have not fully vaporised their liquid component.

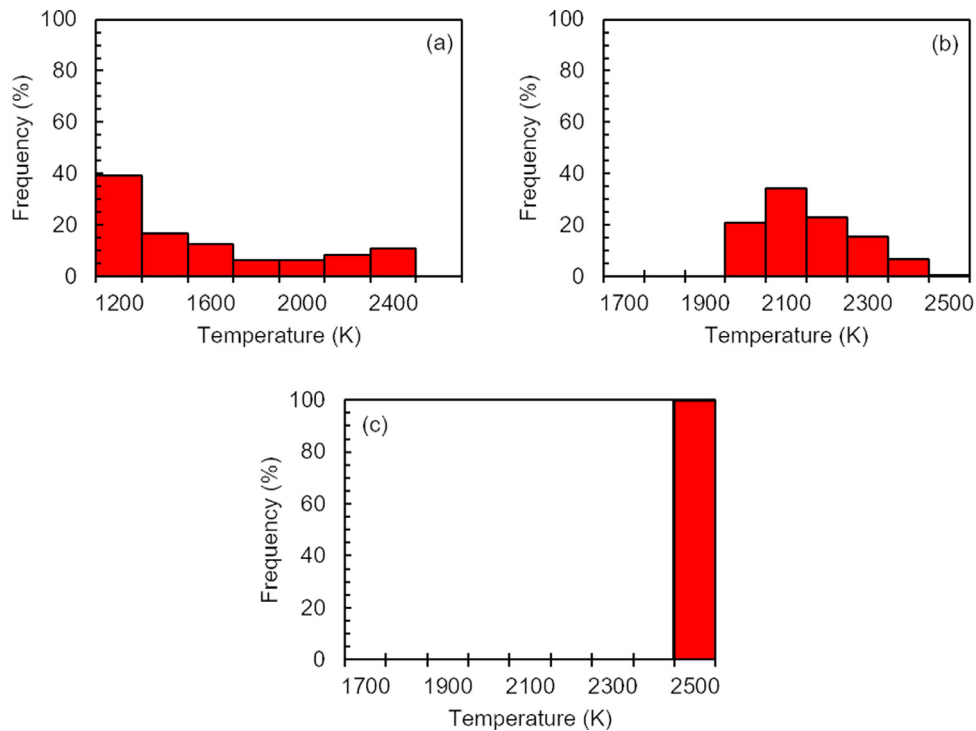


Fig. 10. Particle temperature distribution predicted from the Ranz – Marshall (a), Kavanau (b) and compressible (c) correlations at a standoff distance of 85 mm.

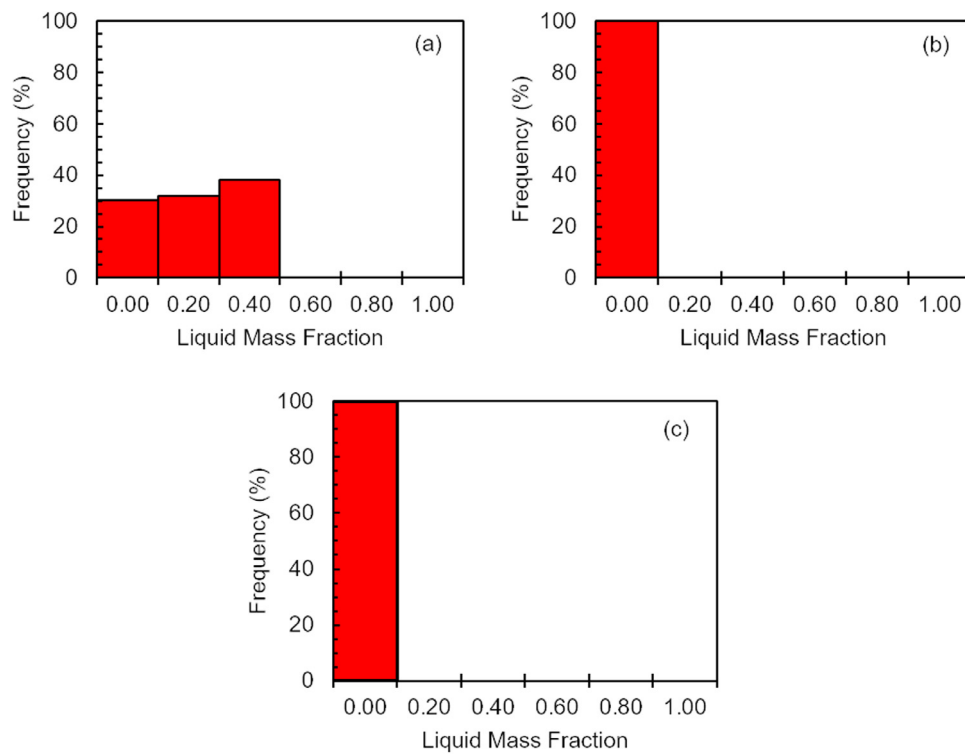


Fig. 11. Particle liquid mass fraction distribution predicted from the Ranz – Marshall (a), Kavanau (b) and compressible (c) correlations at a standoff distance of 85 mm.

Over 50% of suspension droplets contain some degree of volatile material. The high moisture content particles are unlikely to deposit onto the substrate to form a well adhered coating hence, this model suggests a much lower deposition efficiency. Both the Kavanau and the compressible correlations predict that the particles impacting the substrate will not contain any moisture within them.

Fig. 12(a), (b) and (c) shows the inflight particle velocity distribution predicted from the Ranz–Marshall (a), Kavanau (b) and

the compressible (c) correlations at 85 mm from the nozzle exit. It can be seen that both the Kavanau and the compressible correlation provide a very similar velocity distribution with the particle velocity spanning 800 – 900 m/s while the Ranz-Marshall correlation deviates significantly from the other two correlations with a distribution spanning 900 – 100 m/s.

Fig. 13(a), (b) and (c) shows the particle diameter distribution predicted from the Ranz–Marshall (a), Kavanau (b) and the

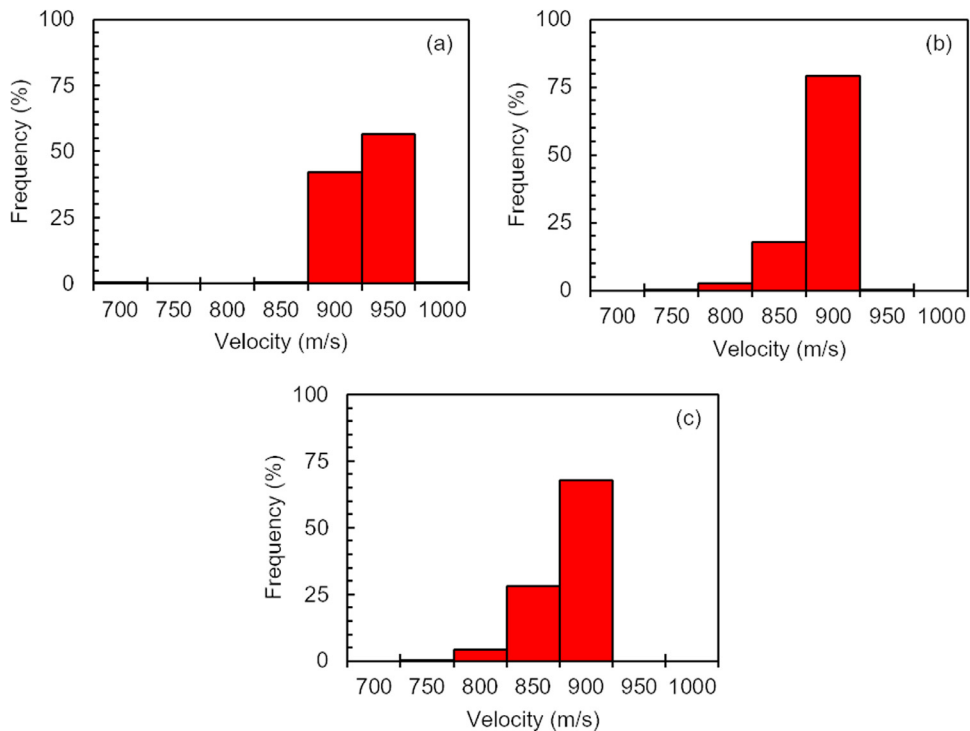


Fig. 12. Inflight particle velocity magnitude distribution predicted from the Ranz – Marshall (a), Kavanau (b) and compressible (c) correlations at a standoff distance of 85 mm.

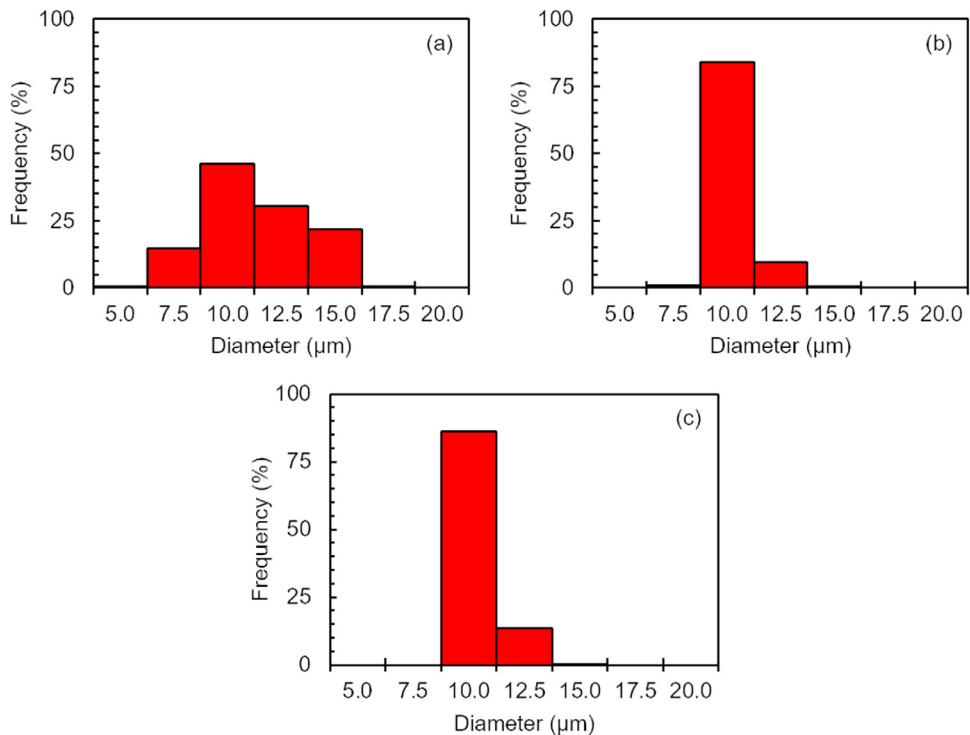


Fig. 13. Inflight particle diameter distribution predicted from the Ranz – Marshall (a), Kavanau (b) and compressible (c) correlations at a standoff distance of 85 mm.

compressible (c) correlations at 85 mm from the nozzle exit. It can be seen that both the Kavanau and the compressible correlation provide a very similar particle diameter distribution with the particle diameters ranging from 7.5 μm – 12.5 μm . Both correlations provide a maximum frequency of 80% – 85% at 10 μm whilst the Ranz-Marshall correlation deviates significantly from the other two models. The Ranz-Marshall correlation predicts a wider distribution of particle diameters that span 7.5 μm – 17.5 μm . The

Ranz-Marshall correlation predicts larger particles as the suspension droplets have a large quantity of liquid within the droplets.

Fig. 14 compares the predicted average inflight temperature for the three Nusselt correlations against that of the experimentally obtained values from the Accuraspray 4.0 system. The Accuraspray 4.0 system takes the average measurement from a volume of approximately 3.2 mm x 10 mm x 25 mm. All average numerical values were taken using the same measurement volume to allow

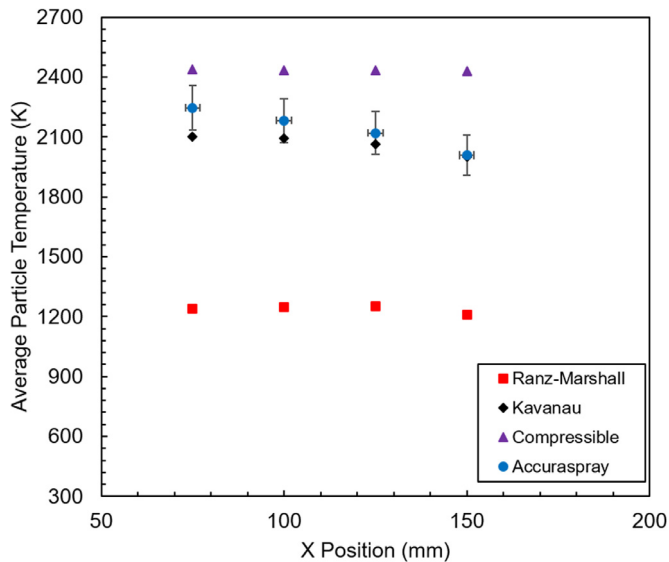


Fig. 14. Comparison of inflight particle temperatures for the three Nusselt correlations against the Accuraspray measurements.

for a direct comparison. It must be noted that the Accuraspray 4.0 measurements correspond to an ensembled average value and do not provide information on the distribution of particle velocities and temperatures. The minimum temperature of particles that the Accuraspray system can detect is approximately 1000°C [36], due to the limited amount of thermal radiation emitted by a cold particle. However, the particle temperature distribution predicted by Fig. 9(b) shows that at the operating conditions employed within this study particle temperatures significantly exceed 1000°C. The ensembled averaged measurements are slightly weighted towards larger sized particles. Mauer et al. [37] compared the particle velocity and temperature measurements taken from DPV-2000 against those obtained from Accuraspray. It was shown that the values taken from DPV-2000 compared well to the measurements obtained from Accuraspray, which suggests that the particle diameter does not have a significant impact on the Accuraspray sensor's accuracy. It can be seen from Fig. 14 that the compressible correlation provides a significant improvement in the particle temperature prediction over the Ranz–Marshall correlation. The compressible correlation accounts for the high Mach number effects on the Nusselt number which the Ranz–Marshall correlation does not. Further improvements to the prediction of inflight average particle temperatures over the compressible correlation is seen by the Kavanau correlation. The Kavanau correlation accounts for the high Mach number effects and the effects of rarefaction on the Nusselt number.

The Ranz–Marshall correlation deviates from the experimental values by an average of 42.9%, the compressible correlation deviates from the experimental values by an average of 12.3% while the Kavanau correlation deviates from the experimental values by an average of 4.8%. The Kavanau correlation hence provides the best overall prediction of inflight particle temperatures. The Ranz–Marshall correlation does not account for the Knudsen number or Mach number effects on the Nusselt number and hence the Ranz–Marshall correlation typically overestimates the Nusselt number within the slip flow regime. A lower heat transfer coefficient allows for more efficient heat transfer from the gas to particles which is accounted for most accurately with the Kavanau correlation. Jadidi et al. [6] compared there SHVOF model using the Ranz–Marshall correlation to that of Accuraspray G3 which underpredicted the particle temperatures by 500 K.

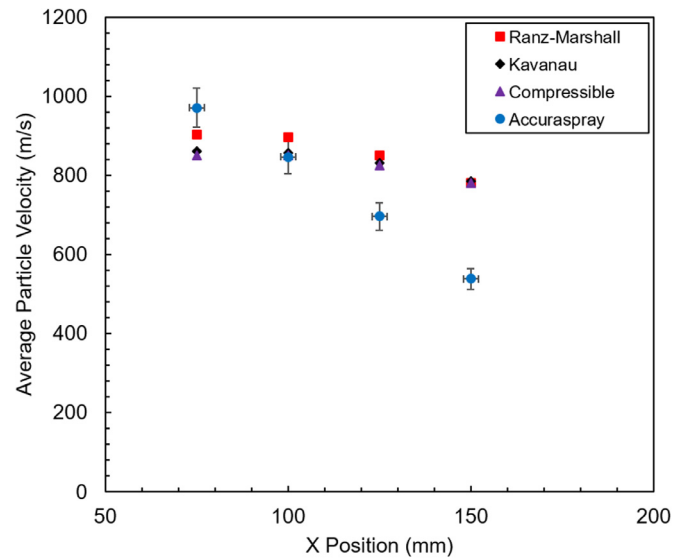


Fig. 15. Comparison of inflight particle velocity for the three Nusselt correlations against the Accuraspray measurements.

Fig. 15 compares the predicted average inflight velocities for the three Nusselt correlations against that of the experimentally obtained values from the Accuraspray 4.0 system. It can be seen from Fig. 15 that all three models compare well with the Accuraspray velocity measurements at low standoff distances. The difference between the Accuraspray measurement and the velocity predicted from the Kavanau correlation is small (1.2%). However, at large standoff distances the error between the Accuraspray measurement and the numerical prediction for the velocity increases. The difference between the experimental and numerical values is as large as 40% at a standoff distance of 150 mm.

There is little sensitivity of the average particle velocity to the Nusselt number is seen at this location. This suggests that the over-prediction may be a result of an underprediction of mixing within the jet. To capture this more accurately a higher-fidelity approach such as large eddy simulation (LES) could be investigated since this has shown improved accuracy for the prediction of single-phase jets. However, this approach is considerably more computationally expensive and application to multiphase flows has been very limited due to the challenges of multi-phase sub-grid scale modelling.

In summary, the flow within SHVOF thermal spray lies outside of the continuum flow regime. This study has shown significant improvements can be made in predictions of the inflight particle temperatures when accounting for the Mach number and the Knudsen number effects. The Ranz – Marshall correlation was derived from measurements of droplets of Reynolds numbers up to 200 and very low Mach numbers. This Ranz–Marshall model was developed for application to spray dryers where the gas operates at very low Mach numbers and was never intended as a one fit model applicable to all flow regimes. As the Mach number increases the heat transfer coefficient reduces. One of the limitations in employing the Ranz–Marshall correlation for SHVOF thermal spray is that it does not account for the effect of the Mach number. In addition to this the model does not account for the effects of rarefaction and hence typically overestimates the Nusselt number outside of the continuum flow regime. It is demonstrated that accounting for the Mach number effects provides a significant improvement in the prediction of inflight particle temperatures. Further additional improvements in the particle temperatures can be seen by also accounting for the Knudsen number effects on the heat transfer coefficient.

5. Conclusion

This study has evaluated the effects of rarefaction on the Nusselt number for application to SHVOF thermal spray. A review of the literature has shown that the Ranz-Marshall correlation has been the sole model employed to SHVOF thermal spray models as this is the standalone model employed within Ansys Fluent. This study has shown that a significant improvement in the prediction of inflight particle temperatures when account for high Mach number effects on the Nusselt number correlation. A further improvement in the prediction of the average inflight particle temperature can be seen by additionally accounting for the effects of rarefaction on the Nusselt number correlation. The Ranz-Marshall correlation provides a good estimate for the Nusselt number in the continuum flow regime at low Mach numbers; however, it overpredicts the heat transfer coefficient within rarefied flow regimes. The compressible correlation which accounts for the high Mach number effects on the Nusselt number provides a significant improvement in prediction of particle temperatures within SHVOF over the Ranz-Marshall correlation. A more accurate correlation still is the Kavanau correlation as this correlation accounts for the high Mach number effects as well as the effects of rarefaction. The model is validated through two colour pyrometry measurements obtained using the Accuraspray 4.0 system. The Ranz-Marshall correlation deviates from the experimental values by an average of 42.3%. The compressible correlation deviates from the experimental values by an average of 12.3%. The Kavanau correlation provides the overall best prediction for the inflight particle temperature, deviating from the experimental values by an average of only 4.8%. It can be concluded that accounting for the effects of rarefaction and high Mach number effects for the suspension allows for a significant improvement in predicting the inflight particle temperatures.

Declaration of competing interest

The authors declare that they have no known competing financial interests or personal relationships that could have appeared to influence the work reported in this paper.

CRediT authorship contribution statement

S. Chadha: Conceptualization, Methodology, Software, Validation, Formal analysis, Investigation, Writing - original draft, Visualization. **R. Jefferson-Loveday:** Conceptualization, Methodology, Resources, Writing - review & editing, Supervision, Project administration. **T. Hussain:** Conceptualization, Methodology, Resources, Writing - review & editing, Supervision, Project administration, Funding acquisition.

Acknowledgement

This work was supported by the [Engineering and Physical Sciences Research Council](#) [EP/N50970X/1]. Access to high performance computing resources provided by the University of Nottingham and HPC midlands plus is gratefully acknowledged.

References

- [1] H. Tabbara, S. Gu, A study of liquid droplet disintegration for the development of nanostructured coatings, *AIChE J.* 58 (11) (2012) 3533–3544.
- [2] M. Mahrukh, A. Kumar, S. Gu, Effects of angular injection, and effervescent atomization on high-velocity suspension flame spray process, *Surf. Coatings Technol.* 302 (2016) 368–382.
- [3] M. Mahrukh, A. Kumar, S. Gu, S. Kamnis, E. Gozali, Modeling the effects of concentration of solid nanoparticles in liquid feedstock injection on high-velocity suspension flame spray process, *Ind. Eng. Chem. Res.* 55 (9) (2016) 2556–2573.
- [4] E. Gozali, M. Mahrukh, S. Gu, S. Kamnis, Numerical analysis of multicomponent suspension droplets in high-velocity flame spray process, *Journal of Thermal Spray Technology* (2014) 940–949.
- [5] M. Taleby, S. Hossainpour, Numerical investigation of high velocity suspension flame spraying, *J. Therm. Spray Technol.* 21 (2012) 1163–1172.
- [6] M. Jadidi, S. Moghtadernejad, A. Dolatabadi, Numerical modeling of suspension hvoof spray, *J. Therm. Spray Technol.* 25 (3) (2016) 451–464.
- [7] J. Oberste Berghaus, B.R. Marple, High-Velocity oxy-fuel (HVOF) suspension spraying of mullite coatings, *J. Therm. Spray Technol.* 17 (5–6) (2008) 671–678.
- [8] Technar, Accuraspray 4.0, (2019). <https://www.technar.com/accuraspray-4-2/> (accessed Aug 21, 2019).
- [9] Ansys Inc, *ANSYS FLUENT V19 R1 User's Guide*; 2019.
- [10] Ansys Inc, *ANSYS FLUENT V19 R1 Theory Guide*; 2019.
- [11] W.E. Ranz, W. Marshall, Evaporation from drops, parts i, *Chem. Eng. Prog.* 48 (1952) 141–146.
- [12] W. Ranz, W. Marshall, Evaporation from drops part ii, *Chemical* 45 (4) (1952) 173–180.
- [13] P.H. Oosthuizen, W.E. Carscallen, *Compressible Fluid Flow*, 1st ed, McGraw-Hill, 1997.
- [14] L.L. Kavanau, J.M. Drake, *Heat Transfer from Spheres to a Rarefied Gas in Subsonic Flow*, California, 1977.
- [15] F.M. Sauer, Convective heat transfer from spheres in a free-molecule flow, *J. Aeronaut. Sci.* 18 (5) (1951) 353–354.
- [16] D.J. Carlson, R.F. Hoglund, Particle drag and heat transfer in rocket nozzles, *AIAA J.* 2 (11) (1964) 1980–1984.
- [17] J.R.M. Drake, G. Backer, Heat transfer from sphere to a rarefied gas in super-sonic flow, *Trans. American Soc. Mech. Eng.* 74 (4) (1952) 1241–1249.
- [18] E. Gozali, S. Kamnis, S. Gu, Numerical investigation of combustion and liquid feedstock in high velocity suspension flame spraying process, *Surf. Coatings Technol.* 228 (2013) 176–186.
- [19] E. Dongmo, R. Gadow, A. Killinger, M. Wenzelburger, Modeling of combustion as well as heat, mass, and momentum transfer during thermal spraying by hvoof and hvsfs, *J. Therm. Spray Technol.* 18 (5–6) (2009) 896–908.
- [20] A. Killinger, M. Kuhn, R. Gadow, High-Velocity Suspension Flame Spraying (HVSFS), a new approach for spraying nanoparticles with hypersonic speed, *Surf. Coatings Technol.* 201 (5) (2006) 1922–1929.
- [21] S. Chadha, R. Jefferson-Loveday, T. Hussain, Effect of nozzle geometry on the gas dynamics and evaporation rates of suspension high velocity oxy fuel (SHVOF) thermal spray: a numerical investigation, *Surf. Coatings Technol.* 371 (15) (2019) 78–89.
- [22] S. Chadha, R. Jefferson-Loveday, F. Venturi, T. Hussain, A computational and experimental investigation into radial injection for suspension high velocity oxy-fuel (SHVOF) thermal spray, *J. Therm. Spray Technol.* 28 (6) (2019) 1126–1145.
- [23] E. Dongmo, A. Killinger, M. Wenzelburger, R. Gadow, Numerical approach and optimization of the combustion and gas dynamics in high velocity suspension flame spraying (HVSFS), *Surf. Coatings Technol.* 203 (15) (2009) 2139–2145.
- [24] A. Farrokhpahan, T. Coyle, J. Mostaghimi, Numerical study of suspension plasma spraying, *J. Therm. Spray Technol.* 26 (1–2) (2016) 12–36.
- [25] R.D. Reitz, Modeling atomization processes in high-pressure vaporizing sprays, *At. Spray Technol.* 3 (4) (1987) 309–337.
- [26] W.E. Ranz, Some experiments on orifice sprays, *Can. J. Chem. Eng.* 36 (4) (1958) 175–181.
- [27] S.V. Apte, K. Mahesh, T. Lundgren, Accounting for finite-size effects in simulations of disperse particle-laden flows, *Int. J. Multiph. Flows* 34 (3) (2008) 260–271.
- [28] C.T. Crowe, Drag coefficient of particles in a rocket nozzle, *AIAA J.* 5 (5) (1967) 1021–1022.
- [29] C.T. Crowe, J.D. Schwarzkopf, M. Sommerfeld, Y. Tsuji, Clayton t, *Multiphase Flows with Droplets and Particles*, 2nd ed, CRC Press, 2012.
- [30] A. Nastic, B. Jodoin, Evaluation of heat transfer transport coefficient for cold spray through computational fluid dynamics and particle in-flight temperature measurement using a high-speed ir camera, *J. Therm. Spray Technol.* 27 (8) (2018) 1491–1517.
- [31] Y.-C. Liu, L.-S. Chao, Modified effective specific heat method of solidification problems, *Mater. Trans.* 47 (2006) 2737–2744.
- [32] P. Lamberg, R. Lehtiniemi, A.-M. Henell, Numerical and experimental investigation of melting and freezing processes in phase change material storage, *Int. J. Therm. Sci.* 43 (3) (2004) 277–287.
- [33] A. Akbarzari, S. Amiri, O. Bamber, J. Grenon, M. Choquet, L. Pouliot, Improvement of online diagnostic system to monitor in-flight particles in thermal spray processes, in: *International Thermal Spray Conference; JTST*, 2019 pp. 957–964.
- [34] P. Gougeon, C. Moreau, V. Lacasse, M. Lamontagne, I. Powell, A. Bewsher, A new sensor for on-line diagnostics of particles under thermal spraying conditions, *Adv. Proc. Tech.* 6 (1994) 199–210.
- [35] S. Zimmermann, E. Vogli, M. Kauffeldt, M. Abdulgader, B. Krebs, B. Rütther, K. Landes, J. Schein, W. Tillmann, Supervision and measuring of particle parameters during the wire-arc spraying process with the diagnostic systems accuraspray-g3 and Ida (Laser-Doppler-Anemometry), *J. Therm. Spray Technol.* 19 (4) (2010) 745–755.
- [36] Technar, Accuraspray 4.0 User Manual - Online Monitoring of Thermal Spray Processes for the Shop Floor, Saint-Bruno-de-Montarville, 2019.
- [37] G. Mauer, R. Vaßen, D. Stöver, Comparison and applications of DPV-2000 and accuraspray-g3 diagnostic systems, *J. Therm. Spray Technol.* 16 (3) (2007) 414–424.
- [38] R.H. Perry, D.W. Green, *Perry's Chemical Engineers' Handbook*, McGraw-Hill, 2008.